Applied Thermal Engineering 130 (2018) 1156–1162

Contents lists available at ScienceDirect

Applied Thermal Engineering

journal homepage: www.elsevier.com/locate/apthermeng

Research Paper

CO_2 footprint reduction and efficiency increase using the dynamic rate in overhead power lines connected to wind farms

A. Arroyo *, P. Castro, M. Manana, R. Domingo, A. Laso

University of Cantabria, Department of Electrical and Energy Engineering, Av. Los Castros s/n., 39005 Santander, Spain

HIGHLIGHTS

- Method to obtain an economic and environmental scenario for wind energy integration.
- Use of dynamic line rating operation to increase energy evacuated from wind farms.
- Dynamic line rating operation decreases the CO_2 footprint and increases income.
- In 2015 dynamic line rating has saved more than 1100 tonnes of CO_2 and 240,000€.
- Latest 2014 CIGRE Standard using the most accurate unsteady thermal balance is used.

ARTICLE INFO

Article history:
Received 22 May 2017
Revised 29 September 2017
Accepted 20 November 2017
Available online 21 November 2017

Keywords:
CO_2 footprint
Dynamic rate
Ampacity
Sustainable energy systems
Climate change

ABSTRACT

Since the first wind farms began operating in the early 1980s, several important factors have changed in the overall picture of energy politics worldwide.

The total renewable wind energy capacity of Spain currently accounts for more than 20% of the total installed capacity, which makes integration into the grid challenging for wind farm owners as well as electricity transportation and distribution companies. The smart-grid concept, which focuses on real-time monitoring and dynamic rating operation of power lines, is an important component in the solution to these new challenges.

This paper explains how a more efficient operation of energy-generating activities via dynamic rating of the electric grid due to a better knowledge of the main parameters contributes to more clean, renewable energy and decreases the CO_2 footprint.

The dynamic rating operation of a Spanish overhead power line is analysed, and different scenarios are studied. The dynamic rate achieved in 2015 has saved more than 1100 tonnes of CO_2 and has generated over 240,000 € of extra income. This dynamic rating operation also increased the actual annual energy generated from 231.5 GW h to 834.7 GW h with only a 2% greater loss along the line due to Joule and magnetic effects.

© 2017 Elsevier Ltd. All rights reserved.

1. Introduction

Since the first wind farms began operating in the early 1980s, several important factors have changed in the overall picture of energy politics worldwide. The globalization of energy strategies, technological and digital improvements, better knowledge of energy conservation and efficiency, the new active role of customers in the energy market and an increasing commitment to the fight against climate change have created synergies to reduce negative environmental impacts from daily human activity [1].

This paper explains how more efficient operation of the electric grid due to a better knowledge of the main parameters contributes to cleaner and more renewable energy and decreases the CO_2 footprint of energy-generating activities [2,3].

Based on the goal of a safe and continuous supply of electricity, the integration of a variable and non-predictable source of energy into an electric system is complex. When the total amount of renewable wind energy capacity exceeds 20% of the total installed capacity of a country, as is the case in Spain [4], this integration becomes challenging for wind farm owners as well as electricity transportation and distribution companies [5]. Fig. 1 shows the evolution of the annual installed wind power and cumulative annual installed wind power in Spain over the last 20 years,

* Corresponding author.
E-mail address: arroyoa@unican.es (A. Arroyo).

https://doi.org/10.1016/j.applthermaleng.2017.11.095
1359-4311/© 2017 Elsevier Ltd. All rights reserved.

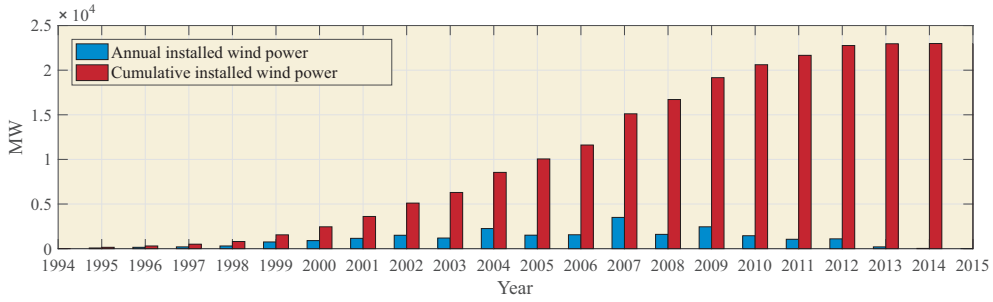

Fig. 1. Annual and cumulative installed wind power in Spain.

according to data obtained from the Spanish Wind Energy Association (AEE) [6–8].

Several problems affect wind energy integration. First, backup power plants are needed to ensure electricity availability, and the wind source is significantly variable. The construction of new powerline infrastructure or the adaptation of existing infrastructure to connect new renewable energy with consumers presents another challenge [9]. The difficulty of creating new lines when a wind farm is built or repowered makes it practically impossible to consider this option because of environmental and legal issues [10,11]. This process can take over 15 years from the first studies to the end of the project, and the cost of creating new energy infrastructure is formidable [12]. Thus, the smart-grid concept, which focuses on real-time monitoring and dynamic rating operation of power lines, is the best option for resolving these problems.

The dynamic rating operation is beginning to be widely used to face several problems like the wind energy integration as can be seen in the reviewed literature [13]. However, there are no studies of this integration being monitored for long periods of time and presenting the specific benefits of this operation in economic and environmental ways. Previous works have partially addressed economic benefits of dynamic rating operation [14]. In order to analyse the complete economic and environmental scenario, the calculation of the line losses must be done. In this paper a new methodology combining thermal and electrical line models is used to obtain this scenario. Additionally, none paper has reported CO_2 saving studies due to a dynamic rating operation, so an estimation of the CO_2 reduction is also presented.

2. Dynamic rating operation

The conductor static rate is the maximum electrical current that a conductor can continuously carry without deterioration. This rate is calculated under notably constrained conditions for the conductor and its environment. The conditions result in rather conservative load values and low-efficiency grids.

The dynamic rate is a result of studies on increasing power line capacity, which is defined as the maximum electrical current that a conductor can continuously carry before deterioration (ampacity), considering the dynamic environmental conditions.

The dynamic rate is limited by several factors, namely, the conductor structure and design, the surrounding environmental conditions, and the line operating conditions. Thus, the conductor dynamic rate considers the variability of the grid and its surroundings (ambient temperature, solar radiation, wind, etc.) [15]. If different conductor cooling and heating processes are measured in real time, the maximum instantaneous current can be used (dynamic rate or ampacity) without reaching the maximum allowable conductor temperature. Hence, the dynamic rate is considered a more efficient control parameter for the power grid than the static rate.

The working parameters should be measured or estimated using different methods (deterministic or probabilistic methods) to calculate the ampacity. CIGRE TB 601 [16] and IEEE 738 [17] are standards that describe the algorithms used to estimate the ampacity and temperature of a conductor [18].

3. Thermal and electrical model

The studied electrical system is composed of the wind farms where electricity is produced and the electrical transmission lines that carry electricity and loads. The environmental parameters are measured using a weather station in the electrical tower, the main electric parameters are measured using a power quality analyser (PQA) in the electrical substation, and the conductor temperature is measured using a temperature measurement sensor (TMS), which is attached to the conductor (Fig. 2).

3.1. Thermal model

The thermal behaviour of an overhead conductor is obtained in terms of the balance of gained and lost heat because of the weather conditions surrounding the conductor and its electrical load [19]. The main sources of gained heat is Joule heating P_j, which includes magnetic effects P_m, and solar radiation P_s. The principal sources of lost heat are convection P_c and cooling radiation P_r to the surroundings.

Fig. 3 shows a scheme of the main electricity parameters for an overhead conductor.

The detailed expressions used to calculate the thermal balance are obtained from the standard CIGRE Dec. 2014 [16] as follows:

Joule Heating (P_j)

The Joule heating gain per unit length for conductors is written as follows:

$$P_j = R_{ac} I^2 \ [\mathrm{W/m}] \tag{1}$$

$$R_{ac} = k_{sk} R_{dc} \ [\Omega/\mathrm{m}] \tag{2}$$

where R_{ac} is the alternating current resistance per unit length at temperature T, I is the RMS conductor current, k_{sk} is the skin effect factor and R_{dc} is the direct current resistance per unit length at temperature T.

The conductor resistance R_{dc} varies with temperature. Thus, the resistivity of a material ρ at any temperature T is expressed as follows:

$$\rho = \rho_{20}\left[1 + \alpha_{20}(T-20) + \zeta_{20}(T-20)^2\right] \ [\Omega\mathrm{m}] \tag{3}$$

where ρ_{20}, α_{20} and ζ_{20} are the resistivity and the linear and quadratic temperature coefficients at 20 °C, respectively.

Thus, the direct current resistance variation R_{dc} due to the temperature increment is written as follows:

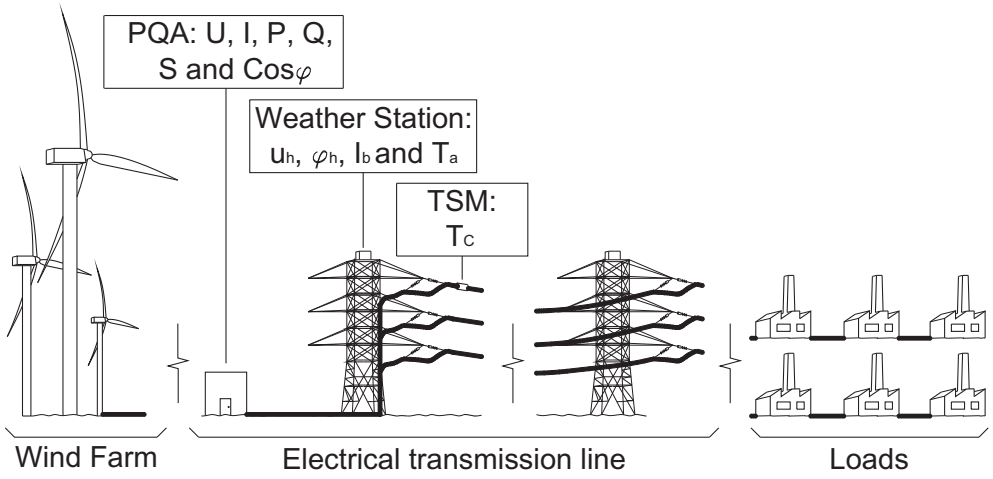

Fig. 2. System description.

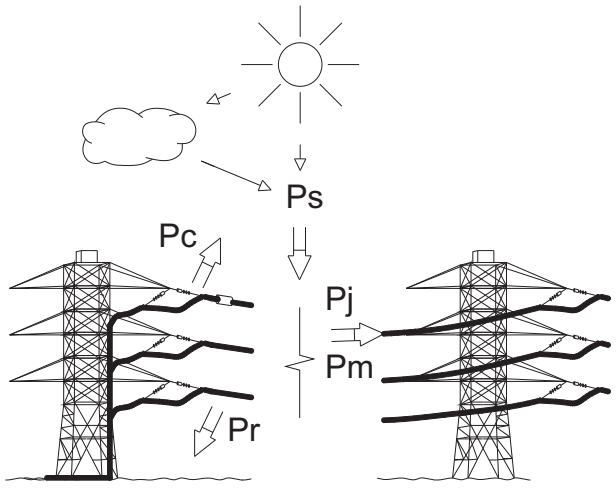

Fig. 3. Overhead conductor heating and cooling.

$$R_{dc} = \frac{\rho}{S}\ [\Omega/\mathrm{m}] \tag{4}$$

where S is the conductor section.

Magnetic Heating (P_m)

A steel-cored conductor causes heating in the steel core (P_{core}) as well as heating due to the redistribution of current densities in the layers of non-ferrous wires (P_{redis}).

$$P_m = P_{core} + P_{redis}\ [\mathrm{W/m}] \tag{5}$$

The magnetic effects are relevant only for steel-cored conductors with one or three aluminium layers and high current densities.

Solar Heating (P_s)

The solar heating per unit length is estimated by the standard as follows:

$$P_s = \alpha_s D I_t = \alpha_s D\left[I_b\left(\sin(\eta) + \frac{\pi}{2}F\sin(H_s)\right) + I_d\left(1 + \frac{\pi}{2}F\right)\right]\ [\mathrm{W/m}] \tag{6}$$

where α_s is the absorptivity of the conductor surface, I_t is the global radiation intensity, D is the outside diameter of the conductor, η is the angle of the solar beam with respect to the axis of the conductor, F is the albedo, H_s is the solar altitude, I_d is the diffuse sky radiation to a horizontal surface, and I_b is the direct solar radiation on a surface normal to the sun's beam.

Convective cooling (P_c)

The convective heat loss can be expressed as a function of the dimensionless Nusselt number (Nu) as follows:

$$P_c = \pi\lambda_f(T_c - T_a)Nu\ [\mathrm{W/m}] \tag{7}$$

where λ_f is the thermal conductivity of air, T_c is the conductor temperature, and T_a is the ambient temperature. Depending on the type of air flow and the speed and direction of the wind (u_h, φ_h), different Nusselt correlations are used by the standard.

Radiative cooling (P_r)

Applying the Stefan-Boltzmann law, the heat loss from the conductor due to radiation is expressed as follows:

$$P_r = \pi D\sigma_B\epsilon_s\left[(T_c + 273)^4 - (T_a + 273)^4\right][W/m] \tag{8}$$

where σ_B is the Boltzmann constant, and ϵ_s is the emissivity of the conductor.

The simplest approach used to determine the thermal state of the conductor assumes that all variables of influence (wind speed and direction, solar radiation, ambient temperature and current) are constant for an interval of time and when the steady-state thermal equilibrium is reached [20]. This assumption leads to a steady-state balance from which the conductor temperature can be obtained as shown in Eq. (9).

$$P_c + P_r = P_j + P_m + P_s \tag{9}$$

The steady-state assumption does not consider the thermal inertia of the conductor materials, and therefore, all variables of interest must be constant at least during the thermal time constant of the conductor. Certain variables fit this condition (ambient temperature and solar radiation), but the most important variables, which are the wind speed and its direction, have large variabilities and are ill suited to the assumption of steady-state conditions for convection cooling [21]. Thus, a time-dependent analysis offers a more accurate estimation of the thermal behaviour of the conductor [22,23]. If a non-equilibrium thermal balance is assumed, Eq. (9) is transformed into the following:

$$mc\frac{\Delta T}{\Delta t} = P_j + P_m + P_s - P_c - P_r \tag{10}$$

where m is the mass per unit length, c is the specific heat capacity, ΔT is the temperature increment, and Δt is the time increment.

According to the previous explanation, Eqs. 1 and 10 are used in the analysis to calculate the current I,

$$I = \sqrt{\frac{mc\frac{\Delta T}{\Delta t} - P_m - P_s + P_c + P_r}{R_{ac}}} \quad (11)$$

3.2. Electrical model

Fig. 4 shows a single-line diagram of the three-phase system. The electrical transmission line consists of different elements, i.e., step-up and step-down transformers in the electrical substations (T_1 and T_2), electrical towers, and conductors (R_{ac} and X_L).

The generated phase-apparent power of the wind farm $\bar{S}_g$ (point A) is the sum of the phase-apparent power in the electrical transmission line $\bar{S}_z$ (between points A and B) and the useful phase-apparent power in the loads $\bar{S}_u$ (point B).

$$\bar{S}_g = \bar{S}_z + \bar{S}_u \ [\text{VA}] \quad (12)$$

The expression used to calculate $\bar{S}_g$ is written as follows,

$$\bar{S}_g = \bar{U}_g \bar{I}^* \ [\text{VA}] \quad (13)$$

where $\bar{U}_g$ is the phase voltage, and $\bar{I}$ can be written as follows:

- Case A: Real phase current measured by the PQA, $\bar{I}_{PQA}$.
- Case B: Maximum conductor current according to the Static Rate (SR), $\bar{I}_{SR}$ (provided by the conductor manufacturer).
- Case C: Current according to the Dynamic Rate (DR), $\bar{I}_{DR}$ (obtained from Eq. (11)).

The phase-apparent power $\bar{S}_z$ can be obtained as follows,

$$\bar{S}_z = \bar{Z}||\bar{I}||^2 \ [\text{VA}] \quad (14)$$

where $\bar{Z}$ is the complex impedance of the transmission line and is calculated as shown,

$$\bar{Z} = L(R_{ac} + jX_L) \ [\Omega] \quad (15)$$

where R_{ac} is calculated in Eq. (2), L is the line length, and X_L is the inductive reactance per unit length for the conductor.

The useful phase-apparent power in loads $\bar{S}_u$ is given by the following,

$$\bar{S}_u = \bar{U}_u \bar{I}^* \ [\text{VA}] \quad (16)$$

where $\bar{U}_u$ is the useful phase voltage in the loads.

Eqs. (17)–(19) are used to calculate the annual generated $E_{g,tot}$, lost $E_{z,tot}$ and useful $E_{u,tot}$ energy, respectively.

$$E_{g,tot} = m_p \sum_{j=0}^{n} \left(Re(\bar{S}_{g_j}) \frac{\Delta t_j}{60 \cdot 10^9} \right) \ [\text{GW h}] \quad (17)$$

$$E_{z,tot} = m_p \sum_{j=0}^{n} \left(Re(\bar{S}_{z_j}) \frac{\Delta t_j}{60 \cdot 10^9} \right) \ [\text{GW h}] \quad (18)$$

$$E_{u,tot} = m_p \sum_{j=0}^{n} \left(Re(\bar{S}_{u_j}) \frac{\Delta t_j}{60 \cdot 10^9} \right) \ [\text{GW h}] \quad (19)$$

where $Re(\bar{S}_{g_j}), Re(\bar{S}_{z_j})$, and $Re(\bar{S}_{u_j})$ are the generated, lost, and useful active power for the sample j, respectively; m_p is the number of phases, Δt_j is the time increment [minutes], and n is the total number of samples.

Depending on the current in Eqs. 13, 14 and 16, different energy values are obtained:

- Case A: If the real phase current $\bar{I}_{PQA}$ is used, the energy values are $E^{PQA}_{g,tot}, E^{PQA}_{z,tot}$ and $E^{PQA}_{u,tot}$.

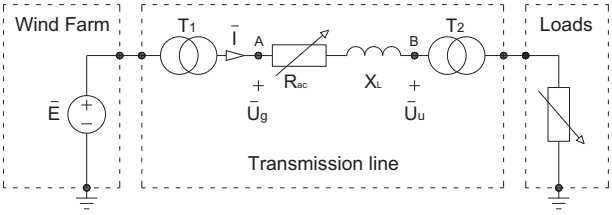

Fig. 4. Electrical model in a single-line diagram view.

- Case B: If the maximum conductor current according to the static rate $\bar{I}_{SR}$ is used, the energy values are $E^{SR}_{g,tot}, E^{SR}_{z,tot}$ and $E^{SR}_{u,tot}$.
- Case C: If the current according to the dynamic rate $\bar{I}_{DR}$ is used, the energy values are $E^{DR}_{g,tot}, E^{DR}_{z,tot}$ and $E^{DR}_{u,tot}$

Eq. (20) is used to study the percentage of loss in each case.

$$\%_{losses} = 100 \cdot \frac{E_{z,tot}}{E_{g,tot}} \quad (20)$$

Finally, four parameters are defined to study the results:

- The total number of hours H_{overSR}, where the real current $\bar{I}_{PQA}$ or dynamic rate $\bar{I}_{DR}$ is greater than the static rate $\bar{I}_{SR}$.
- Energy over static rate,

$$E_{overSR} = E_{u,tot} - E^{SR}_{u,tot} \ [\text{GW h}] \quad (21)$$

where $E_{u,tot}$ can be $E^{PQA}_{u,tot}$ or $E^{DR}_{u,tot}$.

- Tonnes of CO_2 saved per year over the static rate, considering a value of 290 tCO_2/GW h from the Spanish Electricity System (REE) of the year 2015 [24]. The overall value of 290 tCO_2/GW h is obtained dividing the annual emitted CO_2 by the annual generated GW h (Table 1).

$$M_{CO_2} = 290 \cdot E_{overSR} \ [\text{t}] \quad (22)$$

- Extra income per year over the static rate, assuming an average energy price of 62.24 €/MW h. This value is the annual final price of electricity for the free market in Spain (2015) and is obtained from the Nominated Electricity Market Operator of Spain (OMIE) [25],

$$_{income} = 62.24 \cdot 10^3 \cdot E_{overSR} \ [€] \quad (23)$$

4. Data of the specific overhead line

To study the advantages of operating an overhead line under static and dynamic rates, the electrical (U_g, I, S_g, P_g, Q_g and Cos(φ)) and environmental (u_h, φ_h, I_b, T_a and T_c) real-time data were averaged every $\Delta t = 4$ min for an entire year (from January 2015 to December 2015) in a 132-kV overhead line with an LA-110 (94-AL1/22-ST1A)-type conductor [26–28] in northern Spain (Fig. 5). Table 2 describes the variables and equipment used to measure these values. The distance between the starting and ending substations is L = 14.768 km, and the main parameters of the line are summarized in Table 3.

Table 3 shows that the maximum temperature and current of the conductor are 80 °C and 338 A, respectively. These values are based on the method of IEEE 738 [17] and meteorological data: ambient temperature 35 °C; wind speed (perpendicular to the conductor) 0.6 m/s; solar radiation 1078 W/m^2; and solar emissivity and absorptivity of the conductor 0.5. However, the results of this paper are calculated for a maximum conductor temperature of 70 °C to operate with a higher safety margin. Hence, using the method

Table 1
Type of energy, annual generated GW h and annual emitted tCO_2 to calculate the annual relation $tCO_2/GW\ h$ of the year 2015.

Type of energy	Annual Generated GW h	Annual Emitted tCO_2
Renewable and nuclear	150,612	0
Coal	52,789	50,149,589
Oil + Gas	6497	5,257,557
Combined Cycle	29,291	12,154,925
Cogeneration and others	25,449	9,416,313
Waste	3298	791,558
Total	267,936	77,769,941
tCO_2/GW h	290	

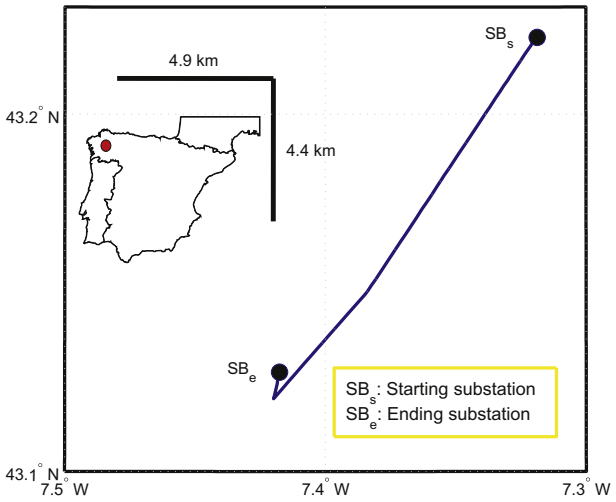

Fig. 5. 132 kV overhead transmission line in northern Spain.

Table 2
Technical data of the measuring equipment.

Measurement	Measuring equipment
Conductor Temperature (T_c)	TMS. 0–120 °C
Conductor current (I)	PQA. 1–5·CT_{Ratio} A ±0.1%
Conductor voltage (U_g)	PQA. 0–900·PT_{Ratio} V ±0.1%
Active power (P_g)	PQA. ±5 kW·CT_{Ratio}·PT_{Ratio} ±0.2%
Reactive power (Q_g)	PQA. ±5kVar·CT_{Ratio}·PT_{Ratio} ±0.2%
Apparent power (S_g)	PQA. ±5 kW·CT_{Ratio}·PT_{Ratio} ±0.2%
CT_{Ratio} and PT_{Ratio}	800/5 A and 132,000/110 V
Frequency (f_g)	PQA. 42.5–62 Hz ±5 mHz
Solar Radiation (I_b)	Pyranometer. 0–1100 W/m^2 ±0.5%
Wind Speed (u_h)	Anemometer. 0–60 m/s ±0.3 m/s
Wind Angle Direction (φ_h)	Anemometer. 0–360° ±2°
Ambient Temperature (T_a)	Thermometer. (−20)–80 °C ±0.3 °C

of IEEE 738 and previous meteorological data, the maximum reachable conductor current according to the static rate $\bar{I}_{SR}$ is 314 A.

5. Results

The data recorded in 2015 for the described line were analysed, and the real current $\bar{I}_{PQA}$ was compared with a static $\bar{I}_{SR}$ and a dynamic $\bar{I}_{DR}$ rating operation during the same period. The studied line was not heavily loaded, and thus, the actual operation was above the static rate for only short periods of time. As an example, the real current $\bar{I}_{PQA}$ (red[1] line), static rate $\bar{I}_{SR}$ (black line) and dynamic rate $\bar{I}_{DR}$ (blue line) are plotted for the month of February 2015 (Fig. 6). As observed, the load was higher than the static rate for only few hours during the month, but the current could have been significantly increased if it had been constantly operated. This result did not occur because of the low demand in the studied line.

Table 3
List of parameters.

Parameters	Description
$D = 0.014$ m	Outside diameter of conductor
$D_1 = 0.006$ m	Core diameter
$L = 14.77$ km	Line length
$y = 557$ m	Altitude
$\varphi = 43$ °	Latitude
$\delta_l = 63$ °	Line angle
$F = 0.1$	Albedo
$N_s = 1$	Clearness Ratio
$\alpha_s = 0.5$	Absorptivity
$\epsilon_s = 0.5$	Emissivity
$m_p = 3$	Number of phases
$m_s = 0.1727$ kg/m	Steel mass per unit length
$m_a = 0.2541$ kg/m	Aluminium mass per unit length
$c_{s,20} = 460$ J/kg K	Specific heat capacity of steel at 20 °C
$c_{a,20} = 880$ J/kg K	Specific heat capacity of aluminium at 20 °C
$\beta_s = 1 \cdot 10^{-4}$ 1/K	Temp. coefficient of steel specific heat capacity
$\beta_a = 3.8 \cdot 10^{-4}$ 1/K	Temp. coefficient of aluminium specific heat capacity
$\lambda_a = 240$ W/mK	Aluminium thermal conductivity
$k_{sk} = 1.025$	Skin factor
$X_L = 0.37$ Ω/km	Conductor inductive reactance per unit length
$\rho_{s,20} = 287.3$ nΩm	Steel resistivity at 20 °C
$\alpha_{s,20} = 4.5 \cdot 10^{-3}$ 1/K	Steel linear resistivity coefficient at 20 °C
$\zeta_{s,20} = 6 \cdot 10^{-6}$ 1/K^2	Steel quadratic resistivity coefficient at 20 °C
$\rho_{a,20} = 28.2$ nΩm	Aluminium resistivity at 20 °C
$\alpha_{a,20} = 4.1 \cdot 10^{-3}$ 1/K	Aluminium linear resistivity coefficient at 20 °C
$\zeta_{a,20} = 8 \cdot 10^{-7}$ 1/K^2	Aluminium quadratic resistivity coefficient at 20 °C
I_{SR}(80 °C) = 338 A	Static rate to 80 °C
I_{SR}(70 °C) = 314 A	Static rate to 70 °C

Table 4 shows and compares the results of the three cases of real current $\bar{I}_{PQA}$, static rating operation $\bar{I}_{SR}$ and dynamic rating operation $\bar{I}_{DR}$ during the entire year. For each case, the annual generated (Eq. (17)), lost (Eq. (18)) and useful (Eq. (19)) energies were calculated and are summarized in Table 4. As observed, notably large increments in useful energy production can be achieved ($E^{SR}_{u,tot} = 535.2$ GW h and $E^{DR}_{u,tot} = 811.1$ GW h) if they are compared with the actual useful energy ($E^{PQA}_{u,tot} = 229.1$ GW h).

Logically, a higher conductor current corresponds to a higher percentage of loss. Thus, the percentage of loss (Eq. (20)) increases from 1.1% in the real case to 1.8% and 2.8% in the static and dynamic rating operations, respectively.

When the real case ($\bar{I} = \bar{I}_{PQA}$) is studied in detail for an entire year (Table 5), we observe that for 424 h, the line was operated over the static rate, and 3.89 GW h of extra energy was evacuated from the connected wind farms (Eq. (21)). Considering the relation of 290 tonnes of CO_2 emission by GW h of fossil fuel electricity production [24], this extra energy led to 1129.5 tonnes of CO_2 conservation in 2015. Assuming that the 2015 averaged energy price was 62.24€/MW h [25], this value indicates 242,402€ of extra income due to the dynamic rating operation.

The real case can be considered a partial dynamic rating operation because $\bar{I}_{PQA}$ was greater than $\bar{I}_{SR}$ for 424 h. Thus, if this partial dynamic rating operation was maintained over the entire year ($\bar{I} = \bar{I}_{DR}$), these benefits could become much more significant. Assuming that the wind farms can deliver the energy rated by the dynamic rating operation, more than 80,000 tonnes of CO_2 and more than 17 M€of extra income could have been saved.

It should be noted that the static and dynamic rates are calculated for a conductor temperature of 70 °C, whereas the maximum

[1] For interpretation of color in Fig. 6, the reader is referred to the web version of this article.

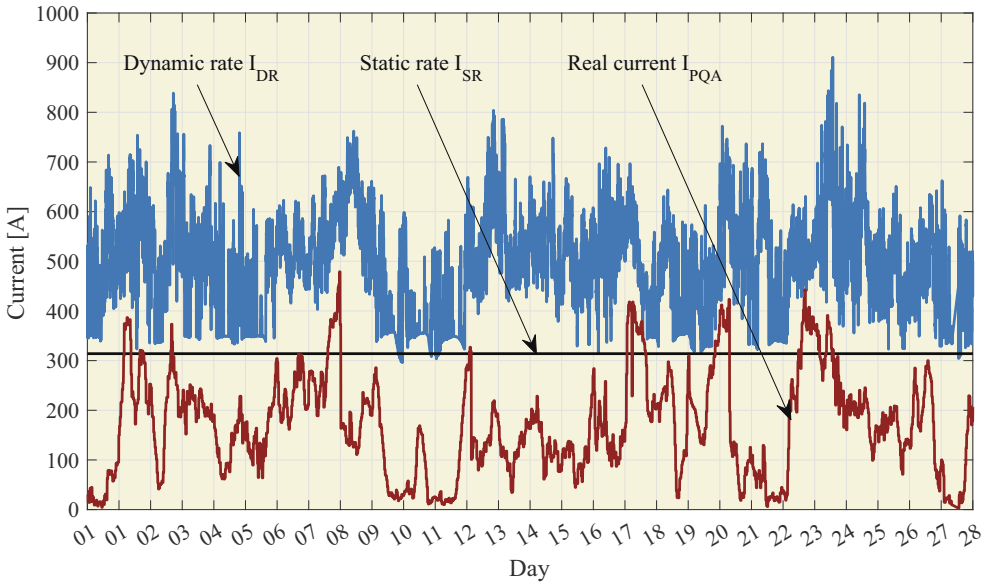

Fig. 6. Comparison of the real current, static and dynamic rate in February 2015.

Table 4
Annual generated, lost and useful energy for each case.

Case	$E_{g,tot}$ GW h	$E_{z,tot}$ GW h	$E_{u,tot}$ GW h	% losses
$A_{(\bar{I}=\bar{I}_{PQA})}$	231.5	2.4	229.1	1.1
$B_{(\bar{I}=\bar{I}_{SR})}$	545.1	9.9	535.2	1.8
$C_{(\bar{I}=\bar{I}_{DR})}$	834.7	23.6	811.1	2.8

Table 5
Results of real and dynamic rating operations vs. the static rate.

	Real case $\bar{I}_{PQA}$ vs. $\bar{I}_{SR}$	Dynamic rate $\bar{I}_{DR}$ vs. $\bar{I}_{SR}$
$H_{over\,SR}$ [h]	424	8385
$E_{over\,SR}$ [GW h]	3.89	257.8
M_{CO_2} [t]	1129	80,000
$€_{income}$	242,402	17,169,761

reachable conductor temperature is 80 °C. Thus, the system works with a safety margin of 10 °C.

6. Conclusions

Renewable-energy grid integration is becoming a daily challenge for grid operators. Improved knowledge of the permitted maximum electric loads enables the electric company to better integrate the energy from wind farms.

In this paper, the dynamic rating operation for an overhead power line was analysed, and different scenarios were studied. The dynamic rating operation is able to increase the annual generated energy of 231.5 GW h to 834.7 GW h with only a 2% greater loss along the line because of Joule and magnetic effects.

In addition, the dynamic rate achieved in 2015 resulted in more than 1100 tonnes of CO_2 savings and more than 240,000€ of extra income. If this dynamic rating operation had been performed over the entire year, the CO_2 savings could have reached 80,000 tonnes of CO_2, and the extra income might have exceeded 17 M€.

Acknowledgments

This work was supported by the Spanish Government under the R+D initiative INNPACTO with reference IPT-2011-1447-920000, the Spanish R+D initiative with reference ENE-2013-42720-R and RETOS RTC-2015-3795-3. The authors also acknowledge support from Viesgo.

References

[1] S. de la Rue, L. Price, T. Zwickel, The full climate change impact of energy consumption and mitigation at the end-use level: a proposed methodology for allocating indirect carbon dioxide emissions, Appl. Energy 159 (2015) 548–559, https://doi.org/10.1016/j.apenergy.2015.08.055.
[2] T. Capuder, H. Pandzic, I. Kuzle, D. Skrlec, Specifics of integration of wind power plants into the croatian transmission network, Appl. Energy 101 (2013) 142–150, https://doi.org/10.1016/j.apenergy.2012.05.002.
[3] J.G. Olazarri, A.J. Mazon, S. Rementeria, I. Albizu, E. Fernandez. Performance of dynamic line rating systems for wind integration, in: 2015 International Conference on Clean Electrical Power (ICCEP), 2015, pp. 567-573. https://doi.org/10.1109/ICCEP.2015.7177548.
[4] The Spanish electricity system report, 2015 (REE).
[5] I. Gonzalez, A. Zucker, Impact of wind power uncertainty forecasting on the market integration of wind energy in Spain, Appl. Energy 159 (2015) 334–349, https://doi.org/10.1016/j.apenergy.2015.08.104.
[6] Spanish wind energy association technical report (AEE), Eólica, 2016.
[7] Ministerio de Industria, Energía y Turismo. La energía en España, 2014.
[8] S. Ruiz, A. Colmenar, M. Castro, Plans for renewable energy: an application to the Spanish case, Renewable Energy 43 (2012) 322–330, https://doi.org/10.1016/j.renene.2011.11.033.
[9] C.J. Wallnerström, Y. Huang, L. Söder, Impact from dynamic line rating on wind power integration, IEEE Trans. Smart Grid 6 (1) (2015) 343–350, https://doi.org/10.1109/TSG.2014.2341353.
[10] P. Martinez, R. Hewitt, J. Diaz, L. Roman, V. Hernandez, J. Vicente, H. Bressers, C. de Boer, Losing the road map: renewable energy paralysis in Spain and its implications for the EU low carbon economy, Renewable Energy 89 (2016) 680–694, https://doi.org/10.1016/j.renene.2015.12.004.
[11] P. del Rio Gonzalez, Ten years of renewable electricity policies in Spain: an analysis of successive feed-in tariff reforms, Energy Policy 36 (8) (2008) 2917–2929, https://doi.org/10.1016/j.enpol.2008.03.025.
[12] B. Lin, J. Li, Analyzing cost of grid-connection of renewable energy development in china, Renew. Sustain. Energy Rev. 50 (2015) 1373–1382, https://doi.org/10.1016/j.rser.2015.04.194.
[13] E. Fernandez, I. Albizu, M. Bedialauneta, A. Mazon, P. Leite, Review of dynamic line rating systems for wind power integration, Renew. Sustain. Energy Rev. 53 (2016) 80–92, https://doi.org/10.1016/j.rser.2015.07.149.
[14] S. Uski, Estimation method for dynamic line rating potential and economic benefits, Int. J. Electric. Power Energy Syst. 65 (2015) 76–82, https://doi.org/10.1016/j.ijepes.2014.09.034.
[15] CIGRE technical brochure 299. Guide for selection of weather parameters for bare overhead conductor ratings, August 2006.
[16] CIGRE technical brochure 601. Guide for thermal rating calculation of overhead lines, December 2014.
[17] IEEE Std. 738-2012. Standard for calculating the current-temperature relationship of bare overhead conductors, December 2012. https://doi.org/10.1109/IEEESTD.2013.6692858.

[18] A. Arroyo, P. Castro, R. Martinez, M. Manana, A. Madrazo, R. Lecuna, A. Gonzalez, Comparison between IEEE and Cigre thermal behaviour standards and measured temperature on a 132-kV overhead power line, Energies 8 (12) (2015) 1366013671, https://doi.org/10.3390/en81212391.
[19] M.W. Davis, A new thermal rating approach: The real time thermal rating system for strategic overhead conductor transmission lines – Part I: General description and justification of the real time thermal rating system, IEEE Trans. Power Apparat. Syst. 96 (3) (1977) 803–809, https://doi.org/10.1109/T-PAS.1977.32393.
[20] V. Morgan, The thermal rating of overhead-line conductors part I. The steady-state thermal model, Electric Power Syst. Res. 5 (2) (1982) 119–139, https://doi.org/10.1016/0378-7796(82)90033-5.
[21] Cigre technical brochure 498. Guide for application of direct real-time monitoring systems, June 2012.
[22] P. Castro, A. Arroyo, R. Martinez, M. Manana, R. Domingo, A. Laso, R. Lecuna, Study of different mathematical approaches in determining the dynamic rating of overhead power lines and a comparison with real time monitoring data, Appl. Therm. Eng. 111 (2017) 95–102, https://doi.org/10.1016/j.applthermaleng.2016.09.081.
[23] J. Rodriguez, C. Franck, Evaluation of the accuracy of a thermal rating model to estimate the temperature of operational transmission lines, CIGRE Sci. Eng. 4 (2016).
[24] Red Eléctrica Española (REE), CO_2 emissions associated to the power generation 2015, Statistical data of Spanish electrical system, 2016.
[25] Operador del Mercado Ibérico Español (OMIE), Annual final price of electricity for free market in Spain, 2015.
[26] EN 50182:2001, conductors for overhead lines. Round wire concentric lay stranded conductors, 2001.
[27] EN 50189:2000, conductors for overhead lines. Zinc coated steel wires, 2000.
[28] EN 60889:1987, hard-drawn aluminium wire for overhead line conductors, 1987.